Glucose intake hampers PKA-regulated HSP90 chaperone activity

Yu-Chen Chen[1,6], Pei-Heng Jiang[1,6], Hsuan-Ming Chen[1], Chang-Han Chen[1], Yi-Ting Wang[2], Yu-Ju Chen[2], Chia-Jung Yu[3,4], and Shu-Chun Teng[1,5,*]

[1]Department of Microbiology, College of Medicine, National Taiwan University, Taipei, Taiwan

[2]Institute of Chemistry, Academia Sinica, Taipei, Taiwan

[3]Department of Cell and Molecular Biology, College of Medicine, Chang Gung University, Tao-Yuan, Taiwan

[4]Department of Thoracic Medicine, Chang Gung Memorial Hospital, Linkou, Tao-Yuan, Taiwan

[5]Center of Precision Medicine, National Taiwan University, Taipei, Taiwan

[6]These authors contributed equally to this article.

[*]Address correspondence to:

Shu-Chun Teng, Department of Microbiology, College of Medicine, National Taiwan University, No. 1, Sec. 1, Jen-Ai Road, Taipei, 10051, Taiwan; Tel: (886) 2-23123456 ext. 88294; Fax: (886) 2-23915293; E-mail: shuchunteng@ntu.edu.tw

21 **Running Title: A crosstalk between two hallmarks of aging - nutrient sensing**

22 **and proteostasis**

23

Abstract

Aging is an intricate phenomenon associated with the gradual loss of physiological functions, and both nutrient sensing and proteostasis control lifespan. Although multiple approaches have facilitated the identification of candidate genes that govern longevity, the molecular mechanisms that link aging pathways are still elusive. Here, we conducted a quantitative mass spectrometry screen and identified all phosphorylation/dephosphorylation sites on yeast proteins that significantly responded to calorie restriction, a well-established approach to extend lifespan. Functional screening of 135 potential regulators uncovered that Ids2 is activated by PP2C under CR and inactivated by PKA under glucose intake. *ids2Δ* or *ids2* phosphomimetic cells displayed heat sensitivity and lifespan shortening. Ids2 serves as a co-chaperone to form a complex with Hsc82 or the redundant Hsp82, and phosphorylation of Ids2 impedes its association with chaperone HSP90. Thus, PP2C and PKA orchestrate glucose sensing and protein folding to enable cells to maintain protein quality for sustained longevity.

Introduction

Aging is a complex process in which cells gradually lose their ability to execute regular functions and organs show increased susceptibility to disease (1). The causes of aging have been attributed to nine hallmarks (2). However, crosstalk between these hallmarks is rare. Calorie restriction (CR) is the most effective intervention known to extend lifespan (3), improve organism function, and retard cell senescence in a variety of species from yeast to mammals (3-6). CR delays the onset and/or reduces the incidence of many age-related diseases, including cancer, diabetes, and cardiovascular disorders (7, 8).

Budding yeast has been perceived as an advantageous model to conveniently examine and isolate new components in aging-related pathways. In yeast, CR can be modelled by reducing the glucose concentration of the media from 2% as the *ad libitum* concentration to 0.5% (or lower), resulting in a 30%-40% increase in lifespan (6, 9). Two different lifespan paradigms are established in querying the lifespan of yeast cells: the replicative lifespan (10) and chronological lifespan (CLS). RLS denotes the number of daughter cells that a single mother cell can generate before senescence, representing the division potential of the mother cell (11), whereas CLS refers to the length of time for which yeast cells remain viable in a non-dividing state (12).

CR exerts anti-aging effects by regulating metabolism (13) and enhancing stress resistance (14). These processes down-regulate the amino acid-sensing mTOR and the glucose-sensing PKA signalling pathways (15). Attenuation of Tor1, Sch9, and PKA kinases promotes activation of Rim15 kinase-mediated transcription factors Msn2/4 and Gis1 to increase pathways in glycogen accumulation, antioxidant enzyme formation, heat shock protein expression, and autophagy (16). Moreover, CR-mediated Tor1 repression enhances Snf1 kinase (the mammalian AMP kinase homologue in yeast) (17) to extend CLS by promoting respiration, acetyl-CoA levels, and autophagy (18-21). Although these signalling pathways regulated by CR-modulated phosphorylation have been studied thoroughly, we speculate that there are other unknown regulators remaining to be explored. Here, we developed a screening procedure to discover additional pathways regulated under CR.

Results

A phosphoproteomic screening method identified Ids2 dephosphorylation under CR.

To explore anti-aging mechanisms, we performed mass spectrometry-based quantitative phosphoproteomic profiling to globally define the phosphorylation and dephosphorylation sites of regulated proteins under CR. The triplicate

78 phosphoproteome maps generated from each calorie-restricted or normal
79 glucose-treated sample were annotated with the phosphopeptides of unambiguously
80 identified phosphorylated amino acid sequences (S1a Fig.). Over 2,672 unique
81 phosphopeptides on 949 proteins were identified ($p < 0.05$, S1 Data). The rightward
82 shift in the 2% glucose/0.5% glucose ratio of phosphopeptides in S1b Fig. indicated
83 that the abundance of phosphopeptides decreased under 0.5% glucose, which is in
84 agreement with that many kinases, such as Tor, Sch9, and PKA, were downregulated
85 under CR (15). Among these phosphopeptides, 318 proteins (508 phosphopeptides)
86 showed a 2-fold increase under 0.5% glucose, meaning that these peptides were
87 phosphorylated under a glucose-limited CR environment; 427 proteins (825
88 phosphopeptides) showed a 2-fold decrease under 0.5% glucose, indicating that these
89 peptides were phosphorylated under a glucose-enriched environment; and 113
90 proteins contained both increased and decreased phosphopeptides on the same protein
91 under 0.5% glucose.

92 To discover additional pathways regulated by phosphorylation under CR, we
93 designed an in silico and functional screening procedure (Fig. 1a). We submitted a
94 total of 632 proteins quantified with 2-fold differential phosphorylation to Gene
95 Ontology (GO) analysis (22). Among them, 334 phosphoproteins were annotated to
96 participate in biological processes including glycolysis ($p < 0.01$), cytokinesis ($p <$

97 0.01), signal transduction ($p < 1.0 \times 10^{-3}$), cell communication ($p < 1.0 \times 10^{-3}$),
98 transcription ($p < 1.0 \times 10^{-5}$), and stress response ($p < 1.0 \times 10^{-4}$) (S1c Fig.). Many
99 instances of phosphorylation regulation in our database coincided with the existing
100 CR/nutrient-sensing pathways (23), such as PKA, Tor, and Snf1 (15) (S1d Fig.). In
101 previous studies, CR has been shown to extend lifespan through an increase in
102 respiration (6), augmentation of cellular protection (15), and induction of
103 autophagy (24). Thus, we challenged the deletion strains of 135 candidates in the
104 top categories of the GO analysis with various stresses, including heat shock,
105 oxidative stress, DNA replicative stress, and/or nonfermentable carbon growth. We
106 also verified the efficiency of autophagy by a GFP-Atg8 cleavage assay (25).
107 Phenotypic analyses exhibited that 53 deletion strains showed defective phenotypes
108 (S2 Data and S2 Fig.). Phosphomimetic and/or dephosphomimetic mutations of these
109 53 candidates were generated to verify the functions observed in the deletion strains,
110 and only the *ids2-S148D* phosphomimetic strain displayed a growth defect in heat
111 shock and glycerol (Fig. 1b). According to our mass spectrometry data (S3a Fig.),
112 S148 on Ids2 was identified (Ids2 RRS$\underline{S}^{148}$IQDVQWIR) to be dephosphorylated
113 under CR. The growth defect under CR was observed in *ids2Δ* and *ids2-S148D* cells
114 (Fig. 1c). Moreover, the *ids2-S148D* phosphomimetic strains showed shortened CLS
115 (Fig. 1d). Ids2 is involved in the modulation of Ime2 during meiosis (26); however, it

is a functionally unknown protein in the mitotic cell cycle. We therefore speculated that Ids2-S148 phosphorylation may play an important role in stress response and lifespan control.

PKA phosphorylates Ids2 upon glucose intake, and PP2C dephosphorylates Ids2 under CR.

To verify the CR-mediated Ids2 phosphorylation, Western blot analysis was conducted. Ids2-S148 phosphorylation was found to be decreased under CR (Fig. 2a and S3b Fig.) but not under nitrogen starvation or TOR pathway inhibition (Fig. 2b and S3c Fig.). Based on the PhosphoGRID and pkaPS databases (27), Ids2 RRS<u>S</u>^{148}IQD may be phosphorylated by PKA (score = 1.57). Deletion of one PKA catalytic subunit, *TPK3*, reduced the Ids2 phosphorylation significantly (Fig. 2c), suggesting that Tpk3 may phosphorylate S148. Deletion of *RAS2* or *GPA2*, the two PKA upstream regulators did not affect Ids2 phosphorylation (S3d Fig.), implying that they act in a redundant manner. An in vitro kinase assay demonstrated that GST-Ids2 was phosphorylated by wild-type PKA kinase from the extract of the KT1115 strain (Fig. 2d) or by the bovine heart PKA catalytic subunit C (S3e Fig.) but not by the extract of the PKA kinase-dead strain (Fig. 2d). These results indicated that PKA may directly phosphorylate Ids2-S148.

To determine the phosphatase(s) dephosphorylating Ids2-S148, we examined the phosphorylation levels in the mutants of major phosphatases. The Ids2 phosphorylation level increased in *ptc2Δ ptc3Δ* cells compared with that in the wild-type (Fig. 2e). An in vitro phosphatase assay showed that recombinant Ptc2 removed the S148 phosphorylation (Fig. 2f), indicating that PP2C may directly dephosphorylate Ids2. Moreover, a spotting assay showed that the *ids2-S148A* mutation could rescue the growth defect in the *ptc2Δ, ptc3Δ* and *ptc2Δ ptc3Δ* mutants (Fig. 2g), suggesting that the PP2C phosphatases (28) may dephosphorylate Ids2.

Ids2 interacts with chaperone HSP90 in a phosphorylation-modulated manner.

To understand the molecular mechanism that Ids2 participates in under CR, we searched for its interaction partners via tandem affinity purification (TAP) and mass spectrometry analysis (29). The bead-bound proteins were separated (Fig. 3a), and spectrometry analysis revealed two closely related proteins, Hsc82 and Hsp82 (30), in the yeast HSP90 family (S3 Data). Expression of Hsc82 is higher than that of Hsp82 under normal conditions, suggesting that Hsc82 plays a more prominent role (30). The co-immunoprecipitation assay showed that Hsc82-HA_3 co-precipitated with Ids2-Myc_{13} (Fig. 3b). A yeast two-hybrid analysis revealed that amino acids 92-256 of Ids2 interact with amino acids 272-579 of Hsc82 (S4 Fig.). Immunoprecipitation of

Ids2-S148D with Hsc82 was significantly decreased, while the Ids2-S148A mutation increases the interaction with Hsc82 (Fig. 3c). In addition, the phosphomimetic S148D mutation of purified recombinant Ids2 impaired the Ids2-Hsc82 interaction in the affinity pull-down assay (Fig. 3d), suggesting that the phosphorylation of S148, which is located within the interacting motif (92-256), may inhibit the Ids2-Hsc82 interaction. To examine the interaction between Ids2 and Hsc82 under CR, an overnight culture was refreshed in medium with 2 % or 0.5 % glucose. As expected, CR significantly increased the Ids2-Hsc82 interaction (Fig. 3e).

Ids2 acts as a co-chaperone in the HSP90-mediated protein-folding process.

HSP90 is an essential eukaryotic chaperone with a well-established role in folding and maintenance of proteins that are associated with the cell signalling response, such as kinases and hormone receptors (30). However, the active participation of co-chaperone proteins at various stages of the chaperone folding cycle is crucial for the completion of the folding process (31). Due to the physical interaction between Ids2 and Hsc82, we speculated that Ids2 may function as either a substrate or a regulator of HSP90. Deletion of *HSC82* did not change the stability of Ids2, suggesting that Ids2 may not be a substrate of Hsc82 (S5 Fig.). Many co-chaperones can regulate HSP90 ATPase, an activity essential for its chaperoning

173 action (32, 33). To test whether Ids2 could modulate the ATPase activity of Hsc82,
174 we performed an Hsc82 ATPase assay with increasing concentration of Ids2 or
175 Ids2-S148D. The assay revealed that Ids2 triggers ATPase activity of Hsc82 and
176 phosphorylation of Ids2 attenuates the reaction (Fig. 4a). Hsc82 is required for
177 mitochondrial F1-ATPase assembly (34). The *ids2Δ* and *ids2-S148D* strains displayed
178 a growth defect in glycerol (Fig. 4b), and formed white colonies, which are caused by
179 the loss of mitochondrial function in the W303-1A strain (35) (Fig. 4b), implying that
180 the phosphorylation of Ids2 may hamper the Hsc82 chaperone activity and thereby
181 diminish the mitochondrial function.
182 We next asked whether Ids2 acts as a co-chaperone of HSP90 in the
183 establishment of the HSP90-mediated protein-folding process. A firefly luciferase
184 reporter assay was used to determine the ability of HSP90-dependent protein
185 refolding (36). Western blot analysis revealed that the protein abundance of firefly
186 luciferase was slightly reduced in *ids2Δ* cells compared to that in *hsc82Δ* cells at 30
187 °C; however, luciferase expression was completely lost in *ids2-S148D* cells, while
188 *ids2-S148A* cells expressed an amount of firefly luciferase equivalent to that of the
189 wild-type (Fig. 4c). Meanwhile, firefly luciferase could not be detected in the *ids2Δ*
190 and *hsc82Δ* strains at 37 °C. Since the accumulation of misfolded proteins would
191 result in degradation (36), a mutant HSP90 chaperone or a dissociation of the

chaperone folding network could cause mass accumulation and subsequent degradation of HSP90-dependent substrates. Taken together, these findings further elucidate that Ids2 may act as a co-regulator for the chaperone activity of HSP90. Since *ids2-S148D* cells displayed a more conspicuous defective phenotype than *ids2Δ* cells, constitutive Ids2 phosphorylation may elicit a greater dominant-negative effect on the chaperone response.

Protein aggregates are found in a variety of diseases, including type II diabetes, Parkinson's disease, and Alzheimer's disease (37). In yeast, many cellular protein aggregates form during aging, for example, Gln1 aggregates with HSP90 upon glucose deprivation and cellular aging (38). Thus, we speculated that compromising the function of Ids2 may lead to aggregation of Gln1. We examined the Gln1-GFP localization in *ids2* phosphomimetic mutants under glucose deprivation (Fig. 4d). The number of Gln1 foci in *ids2-S148D* mutants was dramatically increased compared to that in wild-type and *ids2-S148A* strains, implying that Ids2 phosphorylation may trigger Gln1 aggregation through down-regulation of HSP90 activity.

Discussion

Multiple approaches that integrate large genomic and proteomic datasets have facilitated the identification of factors governing longevity. However, crosstalk

211 between these aging pathways is rare. Both nutrient sensing and proteostasis control
212 lifespan. Here, our phosphoproteomic screen mapped 632 yeast proteins containing
213 CR-responsive phosphorylation. Coupled with functional analyses, we identified a
214 co-chaperone protein, Ids2, which is inactivated under glucose intake. The PKA writer
215 and PP2C eraser orchestrate glucose sensing and protein folding, and phosphorylation
216 of Ids2 impedes its association with HSP90. Thus, glucose concentration influences
217 the HSP90 chaperone activity, enabling cells to control protein quality under
218 environmental conditions for sustained longevity (Fig. 5). Our findings are consistent
219 with a previous large-scale analysis of the genetic interaction between HSP90 and
220 Ids2 (39). We predict that Ids2 is a key regulator in promoting cellular tolerance to
221 stress. HSP90 is a conserved protein controlling late protein-folding steps.
222 Interestingly, sequence alignments of Ids2 show a certain degree of sequence
223 similarity across homologues of HSP90 co-chaperones (S6 Fig.), including the S148
224 residue. It will be interesting to learn whether Ids2 homologues in other organisms
225 also control lifespan.

226 Two lines of observation demonstrated that glucose intake modulates HSP90:
227 high-glucose consumption boosts rat Hsp90 expression (40) and PKA-mediated
228 porcine Hsp90α phosphorylation enhances the translocation of endothelial Hsp90α to
229 the cell surface (41). Through this study, we discovered a previously underappreciated

glucose-mediated chaperone regulatory process: glucose concentration controls HSP90 activity by PKA-dependent co-chaperone phosphorylation. Other than glucose consumption, heat shock (42) and oxidative stress (43) have been shown to regulate the PKA pathway. Indeed, heat shock and oxidative stress both hamper Ids2 phosphorylation, suggesting that cells use Ids2 dephosphorylation to stimulate chaperone activity for coping with various stresses.

We revealed that PP2C phosphatase antagonizes the function of PKA to extend lifespan. *S. cerevisiae* encodes seven phosphatases in the type 2C Ser/Thr phosphatase (PP2C) superfamily (Ptc1-Ptc7) (44), and Ptc1, Ptc2 and Ptc3 are negative regulators of MAPK (45). In deficiencies of the MAPK pathway, cells elevate their stress tolerance ability to extend CLS (46). Although currently there is no direct evidence that PP2C may control stress tolerance through the MAPK pathway, our study provides a means by which PP2C governs stress tolerance: PP2C removes PKA-mediated Ids2 phosphorylation to maintain ample chaperone activity.

Finally, what is the role of Ids2 in protein folding at the molecular level? HSP90 forms a homodimeric complex, which consists of an N-terminal nucleotide binding domain (NBD), a middle domain (M), and a C-terminal dimerization domain (CTD) (47). Co-chaperones can bind to specific domains of HSP90 to stabilize its conformation and further modulate its function. For example, yeast Sti1/Hop and

249 human FKBP51 and FKBP52 utilize their tetratricopeptide (TPR) domains to interact
250 with the C-terminal EEVD motif of HSP90 (48) to stabilize chaperones. Moreover,
251 the N-terminal region of co-chaperone Aha1 interacts with the M domain of HSP90 to
252 stabilize its closed state conformation and thereby increase its ATPase activity (49).
253 Our domain mapping results determined that Ids2 also binds to the M domain of
254 HSP90 and stimulates the ATPase activity of HSP90. In addition, Ids2 forms complex
255 with Aha1 in our MS/MS data of the Ids2-TAP complex. Thus, it will be of interest to
256 investigate the different controlling mechanisms and client specificities of Ids2 and
257 Aha1 in modulating HSP90. Much work will be required to understand the
258 mechanistic role of co-chaperone Ids2.
259

260 **Methods**

261 **Plasmids and Yeast Strains**

262 The yeast strains and plasmids used in this study are listed in S4 Data. Standard
263 genetic and cloning methods were used for all constructions. pYES2-Ids2-TAP was
264 generated by ligation of a PCR product from the Ids2-TAP HISMX6 strain into the
265 KpnI-XhoI-treated pYES2. Kanamycin-resistant knockout strains were constructed
266 through the transformation of kanamycin selection cassette fragments derived from
267 PCR of BY4741. pRS306-*ids2* and other yeast integrating plasmids were

PCR-amplified and cloned into pRS306. Single-point or multiple-site mutations were introduced into pRS306-based plasmids by site-directed mutagenesis. The oligonucleotides designed for mutagenesis and double crossover are listed in S4 Data or are available upon request. To generate chromosomal mutants of these genes, the pRS306-based plasmids were linearized by the appropriate restriction enzymes and transformed into the wild-type strain. After confirming the pop-in structure by Southern blot analysis and 5-FOA selection, the *URA3* pop-out mutants were selected and verified by PCR and sequencing. The C-terminal-tagged Gln1 was created by insertion of the PCR products of the GFP-*HIS3* cassette.

Sample Preparation for Phosphopeptide Enrichment

Yeast cells were grown in yeast extract peptone dextrose (YPD) medium (1 % yeast extract, 2 % bacto-peptone) supplemented with 2 % (normal condition) or 0.5 % glucose (calorie-restricted) for 3 hours and then harvested from log-phase growing cultures. Protein samples were extracted and subjected to gel-assisted digestion (50). First, proteins were fixed by sodium dodecyl sulfate-polyacrylamide gel electrophoresis (SDS-PAGE) directly, and the gel was cut into five pieces for trypsin proteolytic digestion. Digested peptides were extracted three times for 30 mins each and completely dried by vacuum centrifugation at room temperature. Then, we used a

287 homemade immobilized metal affinity column for phosphopeptide enrichment (51).
288 An Ultra-Performance LC^{TM} system (Waters) was used for automated purification of
289 phosphopeptides. The Ni^{2+} ions were removed, and the nitrilotriacetic acid resin was
290 activated. The peptide samples from trypsin digestion were re-established in loading
291 buffer and loaded into an activated immobilized metal affinity chromatography
292 column. Finally, the unbound peptides were removed, and the bound peptides were
293 eluted.
294
295 **LC-MS/MS Analysis**
296 The purified phosphopeptides were analyzed in triplicate LC-MS/MS by an
297 LTQ-Orbitrap XL hybrid mass spectrometer interfaced with an Agilent 1100 series
298 HPLC. Survey full-scan MS spectra were acquired in the Orbitrap (*m*/*z* 350–1600)
299 with the resolution set to 60,000 at *m*/*z* 400 and the automatic gain control target at
300 106. The 10 most intense ions were sequentially isolated for an MS/MS scan using
301 collision-induced dissociation and detection in the linear ion trap with previously
302 selected ions and dynamic exclusion for 90 seconds. All the measurements in the
303 Orbitrap were performed with the lock mass option for internal calibration. Raw
304 MS/MS data from the LTQ-Orbitrap were transformed to msm files using
305 RAW2MSM software (version 1.1). The msm files were searched using Mascot

306 (version 2.2.1**)** against the Swiss-Prot *Saccharomyces cerevisiae* database (version
307 54.2, 6493 sequences) with the following exceptions: only tryptic peptides with up to
308 two missed cleavage sites were allowed, the fragment ion mass tolerance was set at 10
309 ppm, and the parent ion tolerance was set at 0.6 Da. Phosphorylation (52) and
310 oxidation (M) were specified as variable modifications. Peptides were considered
311 identified if their Mascot individual ion score was greater than 20 (*p*-0.05). The false
312 discovery rates for Orbitrap data were determined with a Mascot score greater than 20
313 (*p*-0.05). The quantitative analysis of phosphopeptides was performed with the SEMI
314 label-free algorithm (53). The raw data files acquired from the LTQ-Orbitrap were
315 converted into files of the mzXML format by the program ReAdW, and the search
316 results in MASCOT were exported in Extensible Markup Language data (.xml)
317 format. After data conversion, the confident peptide identification results (*p*-0.05)
318 from each LC-MS/MS run were loaded and merged to establish a global peptide
319 information list (sequence, elution time, and mass-to-charge ratio). Alignment of
320 elution time was then performed based on the peptide information list using linear
321 regression in different LC-MS/MS runs followed by correction of aberrational
322 chromatographic shifts across fragmental elution-time domains. The mass
323 spectrometry raw datasets were deposited to the ProteomeXchange Consortium (54)
324 (http://proteomecentral.proteomexchange.org) via the PRIDE partner repository with

the dataset identifier PXD001368 and DOI 10.6019/PXD001368. The quantitation results for phosphopeptides listed in S1 Data were obtained using IDEAL-Q software and further checked manually (55).

Bioinformatics Analysis - Gene Ontology Enrichment Analysis and KEGG Orthology Analysis

To functionally define the genes identified in this study, we performed Gene Ontology (GO), network, and pathway analyses using the PANTHER classification system (22) (http://www.pantherdb.org/). The genes showing a 2-fold change with Bonferroni multiple correction testing were annotated for GO terms. The spatial-compartmental relationship and the genome annotation between the phosphopeptides were defined through the use of KEGG (Kyoto Encyclopedia of Genes and Genomes) orthology, a genomic, biochemical and enzyme-substrate metabolism-based online database developed by the team of Minoru Kanehisa of Kyoto University (56).

Stress Resistance Assay

Yeast cells were first grown overnight in yeast extract peptone (YEP) or synthetic complete(54) glucose medium at 30 °C. Then, cells were re-inoculated into

fresh YEP or SC medium and grown to exponential phase (OD_{600} = 0.5). Tenfold serial dilutions of indicated strains were spotted onto YEP with 2% glucose (YEPD), YEP with 3% glycerol (YEPG), or SC glucose plates containing various concentrations of chemicals: 0.04 % Methyl methanesulfonate (MMS), 100 mM hydroxyurea, 10 mM H_2O_2, 400 mM LiCl, 50 µg/ml hygromycin B (Hyg B), and 5 nM rapamycin, and incubated at 30 °C (normal) or 37 °C (heat shock) for 2-3 days.

Chronological Lifespan Assay

The CLS assay of wild-type, *ids2Δ*, *ids2-S148A* and *ids2-S148D* strains were carried out as previous described (57, 58). Viability at day 3, when the yeast had reached stationary phase, was defined as the point of 100 % survival. Thereafter, aliquots from the culture were diluted according to the estimated survival and plated on YEPD plates every other day. After 3 days of incubation at 30 °C, colony-forming units were calculated. A semi-quantitative CLS spotting assay was also performed as previously described (59). In brief, the same cell numbers from the culture were serially diluted 10-fold and spotted on YEPD plates every 2 days.

Tandem Affinity Purification

Tandem affinity purification of Ids2 was performed as previously described (60) in the protocol from the Yeast Resource Center of the University of Washington. In brief, the BJ2168 pYES2-Ids2-TAP strain was inoculated into 1 litre SC with 2% raffinose and grown to log phase prior to adding galactose to induce protein overexpression. Cells were lysed with lysis buffer (150 mM NaCl, 1 % Nonidet P-40, 50 mM Tris-HCl pH 7.5, and protease inhibitors) and with the use of glass beads and a homogenizer. Then, 250 µL of IgG Sepharose 6 Fast Flow prep in 1:1 slurry in NP-40 was added to the lysate and incubated at 4 °C for 2 hours with gentle shaking. Beads were washed 3 times with lysis buffer and once with TEV cleavage buffer. Fifty units of TEV protease (Thermos) was added, and the solution was incubated overnight. The supernatant was collected, and calmodulin-binding buffer (25 mM Tris-HCl pH 8.0, 150 mM NaCl, 1 mM Mg acetate, 1 mM imidazole, 2 mM $CaCl_2$, 10 mM β-mercaptoethanol, 0.1 % NP-40) and 200 µL of calmodulin sepharose beads (GE Healthcare) were added for a 2-hour incubation at 4 °C. Samples were washed, and the bound proteins were eluted into fractions with calmodulin elution buffer (25 mM Tris-HCl, pH 8.0, 150 mM NaCl, 1 mM Mg acetate, 1 mM imidazole, 20 mM EGTA, 10 mM β-mercaptoethanol, 0.1 % NP-40). The eluents were combined and precipitated with 25 % trichloroacetic acid. The samples were analyzed with 10 %

SDS-PAGE gels and stained with silver stain. Bands were cut out and trypsinized for mass spectrometry analysis.

One-dimensional SDS-PAGE combined nano-LC-MS/MS (GeLC-MS/MS)

To identify the Ids2-TAP interacting proteins, GeLC-MS/MS, one of the targeted proteomics approaches, was applied as described previously (29). Briefly, gel pieces were destained in 50 mM NH_4HCO_3/ACN (3:2, v/v) three times for 25 min each, dehydrated in ACN and dried in a SpeedVac. In-gel proteins were reduced with 10 mM dithiothreitol in 25 mM NH_4HCO_3 at 56 °C for 45 min, allowed to stand at room temperature (RT) for 10 min, and then alkylated with 55 mM iodoacetamide in the dark for 30 min at RT. After the proteins were digested by sequencing grade modified porcine trypsin (1:100; Promega, Madison, WI) overnight at 37 °C, peptides were extracted from the gel with ACN to a final concentration of 50%, dried in a SpeedVac, and then stored at 20 °C for further use. For reverse-phase LC-MS/MS analysis, each peptide mixture was resuspended in HPLC buffer A (0.1% formic acid, Sigma, St. Louis, MO) and loaded into a trap column (Zorbax 300SB-C_{18}, 0.3 × 5 mm, Agilent Technologies, Wilmington, DE) at a flow rate of 0.2 µL/min in HPLC buffer A. The salts were washed with buffer A at a flow rate of 20 µL/min for 10 min, and the desalted peptides were then separated on a 10 cm analytical C_{18} column (inner

399 diameter, 75 μm). The peptides were eluted by a linear gradient of 0−10% HPLC
400 buffer B (99.9% ACN containing 0.1% formic acid) for 3 min, 10−30% buffer B for
401 35 min, 30−35% buffer B for 4 min, 35−50% buffer B for 1 min, 50−95% buffer B
402 for 1 min, and 95% buffer B for 8 min at a flow rate of 0.25 μL/min across the
403 analytical column. The LC setup was coupled online to an LTQ-Orbitrap linear ion
404 trap mass spectrometer (Thermo Scientific, San Jose, CA) operated using Xcalibur
405 2.0.7 software (Thermo Scientific). Full-scan MS was performed using the Orbitrap in
406 an MS range of 400−2000 Da, and the intact peptides were detected at a resolution of
407 30,000. Internal calibration was performed using the ion signal of cyclosiloxane peaks
408 at m/z 536.165365 as a lock mass. A data-dependent procedure was applied that
409 alternated between one MS survey scan and six MS/MS scans for the six most
410 abundant precursor ions in the MS survey scan with a 2 Da window and
411 fragmentation via CID with 35% normalized collision energy. The electrospray
412 voltage applied was 1.8 kV. Both MS and MS/MS spectra were acquired using one
413 microscan with a maximum fill-time of 1000 and 150 ms for MS analysis,
414 respectively. Automatic gain control was used to prevent overfilling of the ion trap,
415 and 5×10^4 ions were accumulated in the ion trap to generate the MS/MS spectra. All
416 the MS and MS/MS data were analyzed and processed using Proteome Discoverer
417 (version 1.4, Thermo Scientific). The top 6 fragment ions per 100 Da of each MS/MS

418 spectrum were extracted for a protein database search using the Mascot search engine
419 (version 2.4, Matrix Science) against the UniProtKB/Swiss-Prot sequence database.
420 The top-six-peaks filter node improved the number of peptides identified with high
421 confidence by reducing the number of peaks in the searched peak lists. This method
422 avoids matching peptide candidates to spurious or noise peaks, thereby avoiding false
423 peptide matches. The search parameters were set as follows: carbamidomethylation (C)
424 as the fixed modification, oxidation (M), N-acetyl (protein), pyro-Glu/Gln (N-term Q),
425 6 ppm for MS tolerance, 0.8 Da for MS/MS tolerance, and 2 for missing cleavage.
426 After database searching, the following filter criteria were applied to all the results: a
427 minimum peptide length of six, a minimum of two unique peptides for the assigned
428 protein, and peptide and protein identification with FDR less than 1% peptide filter
429 were accepted. For precursor ion quantification, Proteome Discoverer was employed
430 using a standard deviation of 2 ppm mass precision to create an extracted ion
431 chromatogram (EIC) for the designated peptide.
432

433 **Antibody Generation and Western Blot Analysis**

434 Cells were grown at 30 °C in YEPD medium. Cell lysates were prepared with
435 lysis buffer (150 mM NaCl, 1 % nonidet P-40, 1 % deoxycholate, 0.1 % SDS, 50 mM
436 Tris-HCl, pH 7.5, and protease inhibitors) or precipitated with trichloroacetic acid. To

generate antibodies, rabbits were boosted with carrier-conjugated phosphopeptides once per month. Pre-immune sera were collected before boosting. Blood was collected every 2 weeks, incubated at 37 °C for 30 mins, and separated via high-speed centrifugation. Clarified serum was incubated at 56 °C for 30 mins to remove complement. The specificity of antibodies was verified by means of peptide dot blot analysis. Images were captured and quantified by a bioluminescence imaging system (UVP BioSpectrum AC Imagine System, UVP).

In Vitro Kinase and Phosphatase Assays

The Ids2 ORF was cloned into the EcoRI and XhoI sites of pGEX-4T-1 for expression of GST-Ids2. A point mutation of Ids2-S148 was created to express GST-Ids2-S148A. Bovine heart catalytic subunit C (C_b) was purchased from Millipore and PKI 6-22 (Millipore) was used as a negative control. PKA was obtained from crude extracts of yeast strain KT1115, and the PKA kinase-dead strain was used as a negative control (61). For the phosphatase assay, the full length Ptc2 and the C terminal-truncated Ptc2 (1-312) sequences were cloned into the BamHI and SalI sites of pGEX-4T-1 for the expression of GST-Ptc2 and GST-Ptc2 (1-312)-kinase-dead, respectively. GST proteins were expressed in the BL21 (DE3) pLysS strain in LB plus Amp and induced with 1 mM isopropyl-1-thio-β-D-galactopyranoside (IPTG) at

37 °C for 3 hours. The GST-tagged proteins were purified with Glutathione Sepharose 4B (GE) in binding buffer (140 mM NaCl, 2.7 mM KCl, 10 mM Na_2HPO4, 1.8 mM KH_2PO4 pH 7.5, 1 % Triton X-100, 10 % glycerol) for 1 hour and eluted with elution buffer (50 mM Tris-HCl, 10 mM reduced glutathione pH 8.0).

The kinase assay was started by mixing different sources of PKA (50 mM extracts from KT1115) with GST-Ids2 substrates in kinase buffer (50 mM potassium phosphate pH 7.5, 0.1 mM EGTA, 0.1 mM EDTA, 15 mM $MgCl_2$, 10 mM β-mercaptoethanol, 100 mM ATP). After 15 min at 30 °C, the samples were analyzed by Western blotting with Ids2 S148 phosphospecific antibodies. For the isotope assay, additional γ-^{32}P-ATP was added to the mixture, and the aliquots were processed according to the phosphocellulose paper method (61).

For the phosphatase assay, phosphorylated Ids2 was generated by incubating GST-Ids2 with bovine heart catalytic subunit C (C_b) in kinase buffer for 15 min at 30 °C. The reaction was stopped by incubating with PKI 6-22 at 30 °C for 10 min. GST-Ptc2 or GST-Ptc2 (1-312) was then added to the mixture for the phosphatase reaction. After 15 min at 30 °C, samples were analyzed by Western blotting with Ids2 S148 phosphospecific antibodies.

Co-immunoprecipitation Assay

W303 strains containing chromosomally-tagged *HSC82*-HA_3 and *IDS2* plasmids

476 (pRS426-*IDS2*-Myc$_{13}$, pRS426-*ids2-S148A*-Myc$_{13}$, or pRS426-*ids2-S148D*-Myc$_{13}$)
477 were grown to exponential phase, and cells were harvested. Pellets were resuspended
478 in lysis buffer (50 mM NaCl, 0.1 % NP-40, 150 mM Tris-HCl pH 8.0) supplemented
479 with protease inhibitors (Roche). Cells were broken by a FastPrep-24 5G
480 Homogenizer (MP biomedical) and supernatants were collected after centrifugation.
481 The supernatants were mixed with either anti-HA (Roche) or anti-Myc (Roche)
482 antibodies, and followed by incubation with protein G Sepharose beads.
483 Immunoprecipitates were washed four times with lysis buffer and then eluted by
484 boiling in sample buffer. Samples were resolved by 7 % SDS-PAGE and analyzed
485 by Western blotting using the appropriate antibodies.
486
487 **Yeast Two-hybrid Analysis**
488 To investigate the interaction between Ids2 and Hsc82, a DNA fragment
489 encoding the full length or N-terminal amino acids of Ids2 was ligated downstream of
490 the Gal4 DNA-binding domain in pGBDU-C1. A fragment encoding the full length or
491 N-terminal amino acids of Hsc82 was inserted in pGAD-C1 downstream of the Gal4
492 DNA-activating domain. The resulting plasmids were transformed into PJ69-4A and
493 Leu$^+$ and Ura$^+$ cells were selected. Cells were restreaked on SC-Leu-Ure-Ade-His
494 glucose plates to inspect the bait-prey reciprocity.

495

496 **His-tagged Metal Affinity Purification Assay**

497 An expression construct bearing Hsc82 with an N-terminal His_6-tag was
498 transformed into *E. coli*. *E. coli* cultures were grown in LB media to an OD_{600} of 0.8
499 and then induced with 0.5 mM IPTG for 4 hours. The His_6-tag proteins were purified
500 with TALON His-tagged Protein Purification Resins (GE) in binding buffer (50 mM
501 Tris-HCl pH 8.0, 100 mM NaCl, 50 mM imidazole, 1 % Triton X-100) for 1 hour and
502 eluted with elution buffer (50 mM Tris-HCl pH 8.0, 250 mM imidazole, 10 %
503 glycerol).

504 For the His_6-Hsc82 pull down assay, purified His_6-Hsc82 were incubated with
505 purified GST-Ids2 or GST-Ids2-S148D in incubation buffer (20 mM Tris-HCl pH 7.5,
506 50 mM NaCl, 5% glycerol, 0.01% Triton X-100, 2 mM DTT) at 4 °C for 1 hour. The
507 reaction was precipitated with TALON His-tagged Protein Purification Resins (GE) at
508 4 °C for 1 hour. After washing three times with incubation buffer, the His_6-tagged
509 Hsc82 and co-purified Ids2 proteins were recovered by elution with imidazole.

510

511 **ATPase Assay**

512 For the ATPase assay, His_6-Hsc82, GST-Ids2, and GST-Ids2-S148D proteins
513 were isolated on appropriate columns (a HisTrap™ FF column for His-tagged

514 proteins and a GSTrap™ FF column for GST-tagged proteins) using AKTA Explorer
515 FPLC (GE Healthcare) and further purified by size exclusion chromatography on a
516 Superdex 200 column (GE healthcare) in 25 mM Hepes pH 7.2, 50 mM NaCl, and
517 5 mM β-mercaptoethanol.

518 The ATPase activity of Hsc82 was measured by using EnzChek phosphate assay
519 kit (Molecular Probes, Inc.) as previously described (33). The His_6-Hsc82 protein
520 (2μM) was incubated with Ids2 or Ids2-S148D protein at 37 °C with 1 mM ATPase
521 buffer (40 mM HEPES pH 7.5, 150 mM KCl, 5 mM $MgCl_2$, 2 mM DTT) .The
522 reactions were incubated for 90 min and then diluted 1:5 into a 100-μl phosphate
523 assay reaction as outlined by the manufacturer's instructions. A standard curve was
524 generated using the inorganic phosphate solution provided by the manufacturer
525 (Molecular Probes, Inc.).

526

527 **In Vivo Chaperone Assay**

528 A pRS316 plasmid containing the *GAL1-10* promoter and the SEL-allele of
529 firefly luciferase (36) was purchased from Addgene and transformed into wild-type,
530 *ids2Δ*, *hsc82Δ, ids2-S148A*, and *ids2-S148D* cells. Cells were inoculated into raffinose
531 medium and cultured overnight prior to 3-hours galactose induction in various
532 temperatures. Protein was precipitated by TCA and Western blot analysis was

533 performed with anti-firefly luciferase antibodies (Genetex).

534

535 **Induction of Gln1 Foci by Glucose Deprivation**

536 Cells with Gln1-GFP expression were inoculated into fresh SC glucose selection

537 medium to 0.3 OD/ml from overnight culture. When cells were regrown to 1 OD/ml,

538 cells were washed with PBS and then resuspended in SC medium without glucose for

539 45 min to induce foci formation. After induction, cells were harvested and fixed with

540 3.7% formaldehyde. Statistical significance was analyzed by the student's t-test using

541 GraphPad Prism 5 (GraphPad Software, Inc.).

542

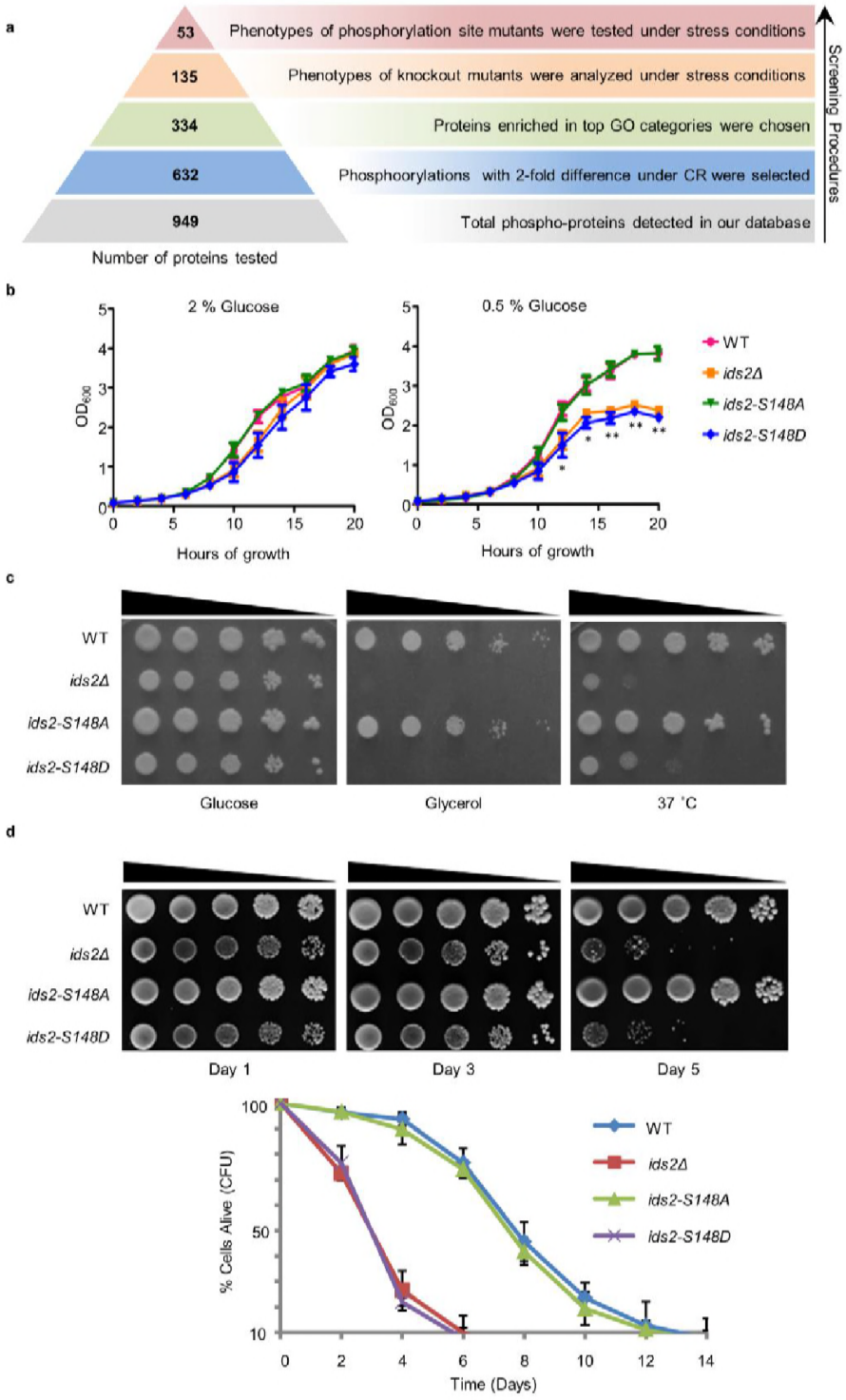

543

544 **Figure 1. Ids2-S148 phosphorylation influences stress tolerance, growth, and**

545 **chronological lifespan.**

546 **a**, A schematic diagram highlights the steps in candidate screening. **b**, Growth curves

547 at 30 °C were monitored in triplicate and represented as the mean ± S.E. (standard

548 errors). **c**, Tenfold serially diluted cells were grown under heat shock (37 °C) in 2 %

549 glucose or at 30 °C in 3 % glycerol. WT and S148D mutants were compared using

550 Student's t-test. *, $p < 0.05$. **, $p < 0.01$. **d**, For the chronological lifespan assay, CFU

551 viability was determined. 10-fold serial dilutions were spotted on YEPD plates.

552 Quantitative CLS assay was assessed in triplicate by colony-forming capacity on

553 YEPD plates.

554

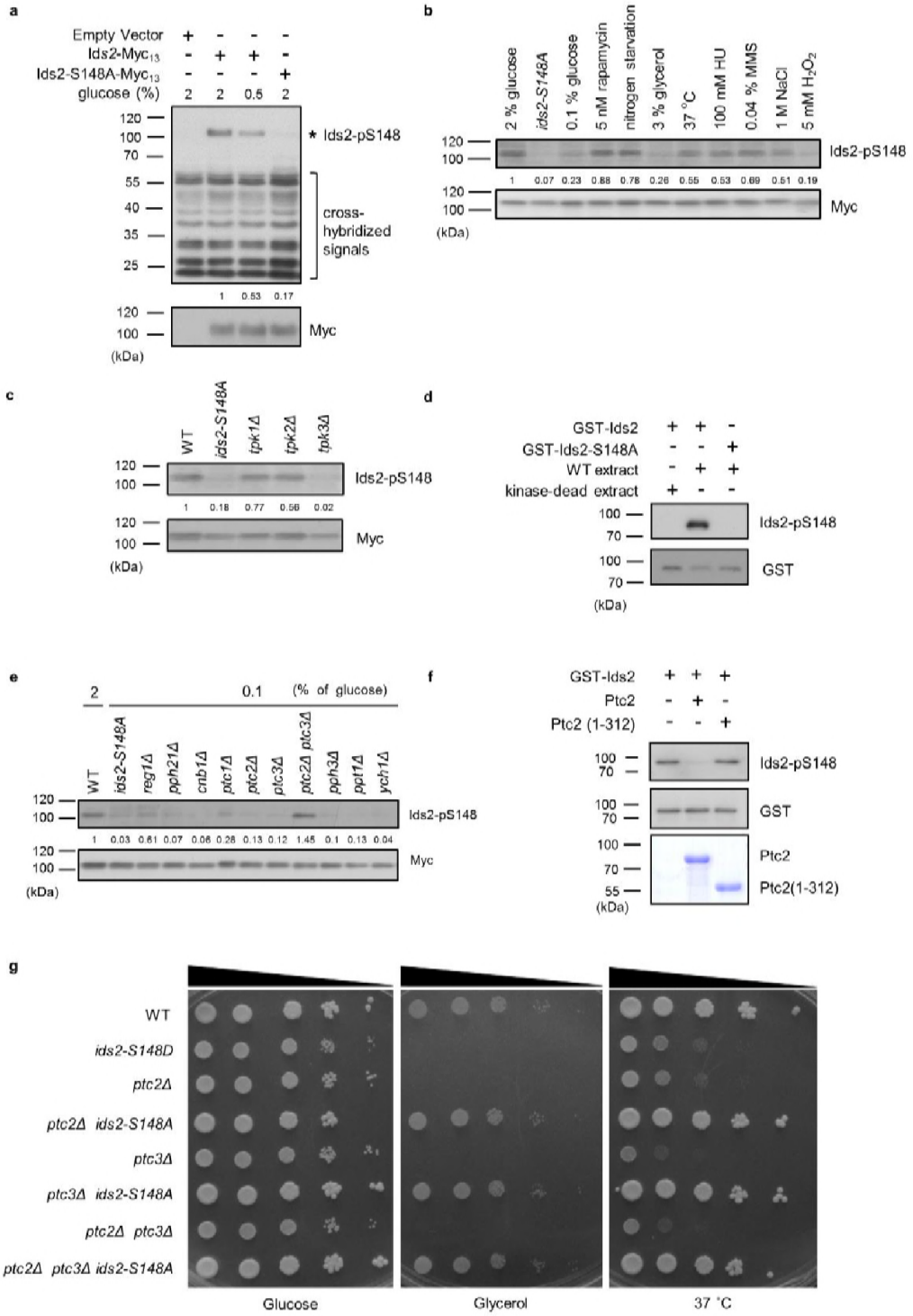

555

556 **Figure 2. PKA and PP2C regulate Ids2-S148 phosphorylation.**

557 **a-c, e,** Strains were transformed with pRS426-Ids2-Myc$_{13}$, and lysates were examined

558 by Western blot analysis with the indicated antibodies. The numbers below are the

559 means of the intensity ratios of Ids2-p148/Myc compared with that of WT treated with

560 2 % glucose. **b**, Overnight cells were refreshed in medium with different treatments

561 for 3 hours. **d**, **f.** In vitro kinase and phosphatase assays were conducted as described

562 in the Methods section. **g**, Cells were spotted in 10-fold dilutions on YEPD or YEPG

563 plates and grown at 30 or 37 ˚C.

564

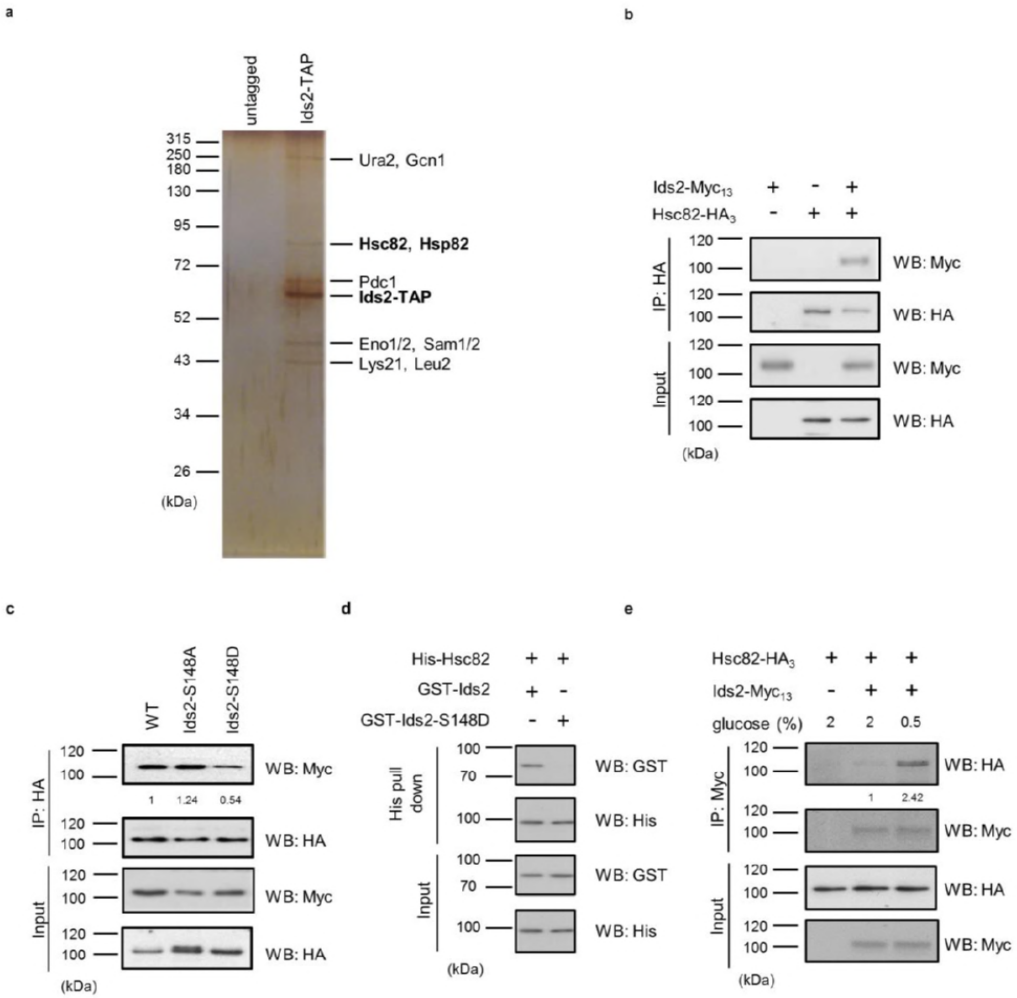

Figure 3. Ids2 interacts with HSP90 families.

a, A silver-stained gel of the affinity-purified Ids2. Both HSP90 families, Hsc82 and Hsp82, were identified by LC-MS/MS analysis. **b**, A co-immunoprecipitation assay was conducted using chromosomal-tagged Ids2-Myc_{13} and Hsc82-HA_3. **c**, Co-immunoprecipitation assay between Hsc82 and Ids2 mutants. The levels of signal compared with that of WT are shown below. **d,** Purified recombinant GST-Ids2 and His_6-Hsc82 proteins were subjected to a His-tagged Metal Affinity Purification assay. **e**, Tagged strains were incubated in 2% (normal) or 0.5% (62) glucose. Ids2-Myc_{13}

574 was used to co-immunoprecipitate Hsc82-HA_3. The numbers below are the means of

575 the intensity ratios of HA/Myc compared with that of WT.

576

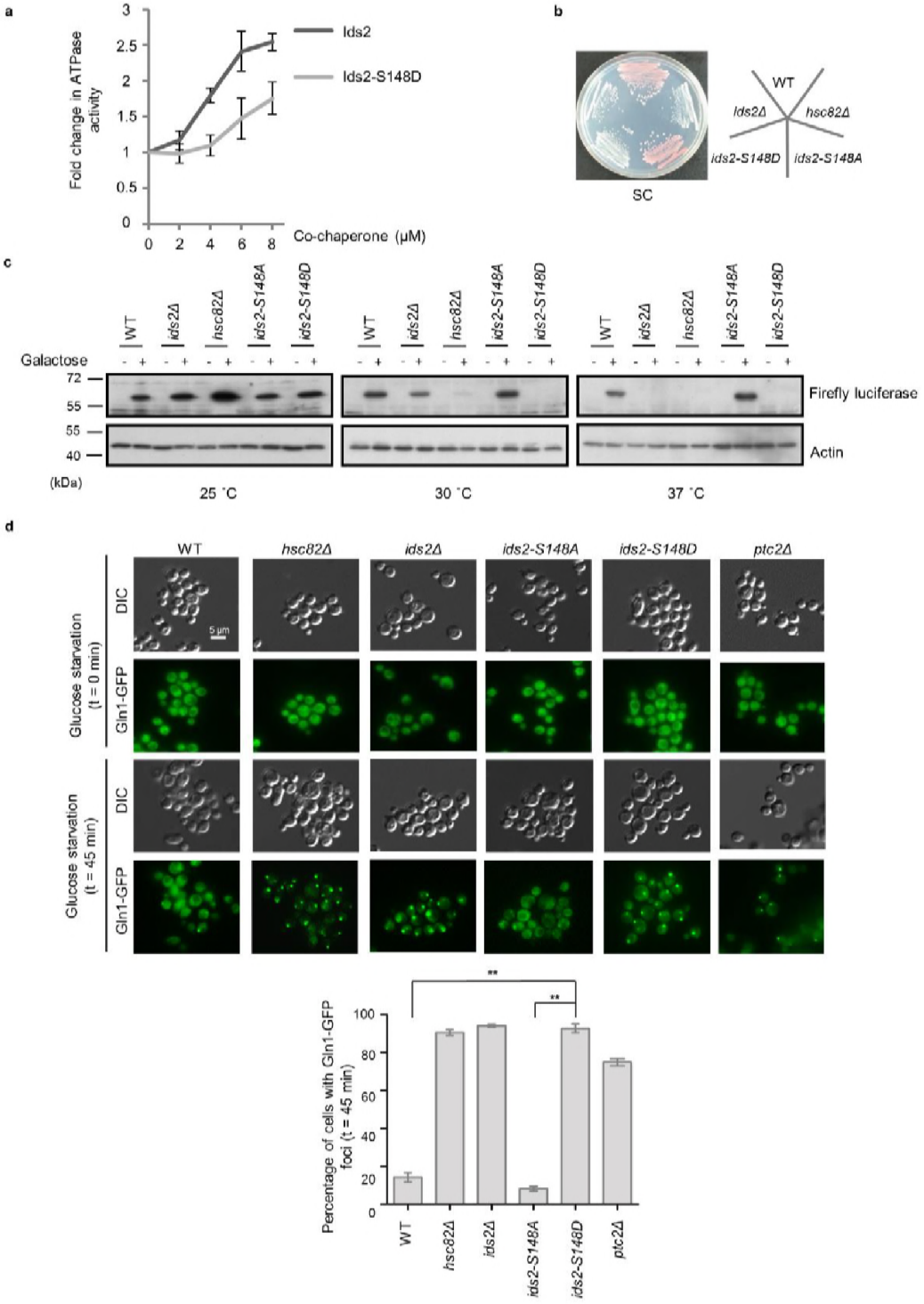

577

578 **Figure 4. Ids2 participates in the HSP90-regulated protein-folding response.**

579 **a,** The purified Hsc82 was mixed with Ids2 or Ids2-S148D, and the ATPase reaction

580 was incubated for 90 min at 37 ˚C. Error bars represent standard deviation calculated

581 from 3 independent experiments. **b**, Cells as indicated were streaked on SC glucose,

582 and the plate image was captured after 3 days. **c**, An in vivo chaperone assay was

583 conducted using an exogenously expressed firefly luciferase, and Western blot

584 analysis was performed. **d**, Endogenously expressed Gln1-GFP in WT and mutant

585 cells was measured after 45 min without glucose. At least 200 cells were counted for

586 each strain (**, $p < 0.01$, Student's t-test, two-tailed).

587

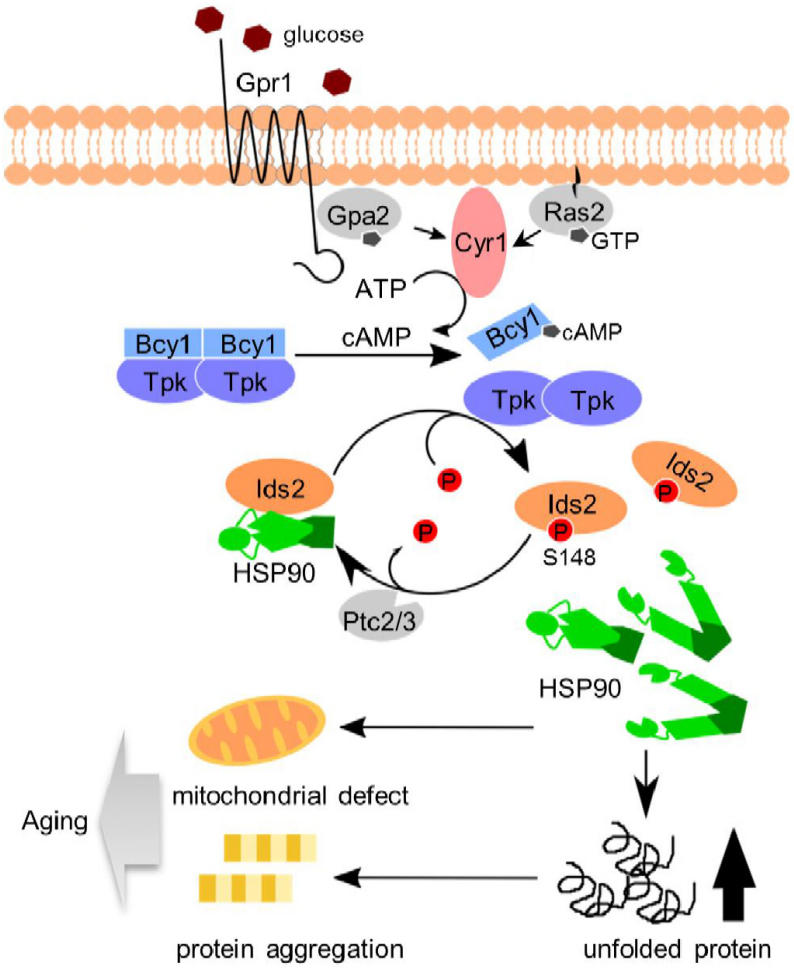

588

589 **Figure 5. A proposed model to describe how glucose intake down-regulates**

590 **chaperone activity and leads to aging.**

591 After glucose ingestion, cells convert ATP to cAMP to activate the PKA pathway.

592 Activated PKA phosphorylates co-chaperone Ids2 to dissociate it from the Hsp90

593 chaperone and reduce chaperone function, eventually leading to protein unfolding,

594 mitochondrial dysfunction and protein aggregation. However, under CR, PP2C

595 removes Ids2 phosphorylation to maintain Hsp90 chaperone function, elevates stress

596 tolerance, and further extends lifespan.

597

598 **References**

599 1. Harman D. The aging process. Proc Natl Acad Sci U S A. 1981;78(11):7124-8.
600 2. Lopez-Otin C, Blasco MA, Partridge L, Serrano M, Kroemer G. The hallmarks
601 of aging. Cell. 2013;153(6):1194-217.
602 3. McCay CM, Crowell MF, Maynard LA. The effect of retarded growth upon the
603 length of life span and upon the ultimate body size. 1935. Nutrition.
604 1989;5(3):155-71.
605 4. de Cabo R, Liu L, Ali A, Price N, Zhang J, Wang M, et al. Serum from
606 calorie-restricted animals delays senescence and extends the lifespan of normal
607 human fibroblasts in vitro. Aging (Albany NY). 2015;7(3):152-66.
608 5. de Cabo R, Carmona-Gutierrez D, Bernier M, Hall MN, Madeo F. The search for
609 antiaging interventions: from elixirs to fasting regimens. Cell. 2014;157(7):1515-26.
610 6. Lin SJ, Kaeberlein M, Andalis AA, Sturtz LA, Defossez PA, Culotta VC, et al.
611 Calorie restriction extends *Saccharomyces cerevisiae* lifespan by increasing
612 respiration. Nature. 2002;418(6895):344-8.
613 7. Mattson MP, Wan R. Beneficial effects of intermittent fasting and caloric
614 restriction on the cardiovascular and cerebrovascular systems. J Nutr Biochem.
615 2005;16(3):129-37.
616 8. Roth GS, Ingram DK, Lane MA. Caloric restriction in primates and relevance to
617 humans. Ann N Y Acad Sci. 2001;928:305-15.
618 9. Lin SJ, Defossez PA, Guarente L. Requirement of NAD and SIR2 for life-span
619 extension by calorie restriction in *Saccharomyces cerevisiae*. Science.
620 2000;289(5487):2126-8.
621 10. Tesch P, Sjodin B, Thorstensson A, Karlsson J. Muscle fatigue and its relation to
622 lactate accumulation and LDH activity in man. Acta Physiol Scand.
623 1978;103(4):413-20.
624 11. Mortimer RK, Johnston JR. Life span of individual yeast cells. Nature.
625 1959;183(4677):1751-2.
626 12. Longo VD, Fabrizio P. Chronological aging in *Saccharomyces cerevisiae*.
627 Subcell Biochem. 2012;57:101-21.
628 13. Kapahi P, Zid BM, Harper T, Koslover D, Sapin V, Benzer S. Regulation of
629 lifespan in Drosophila by modulation of genes in the TOR signaling pathway. Curr
630 Biol. 2004;14(10):885-90.
631 14. Fabrizio P, Pozza F, Pletcher SD, Gendron CM, Longo VD. Regulation of
632 longevity and stress resistance by Sch9 in yeast. Science. 2001;292(5515):288-90.
633 15. Wei M, Fabrizio P, Hu J, Ge H, Cheng C, Li L, et al. Life span extension by
634 calorie restriction depends on Rim15 and transcription factors downstream of

635 Ras/PKA, Tor, and Sch9. PLoS Genet. 2008;4(1):e13.
636 16. Fontana L, Partridge L, Longo VD. Extending healthy life span--from yeast to
637 humans. Science. 2010;328(5976):321-6.
638 17. Orlova M, Kanter E, Krakovich D, Kuchin S. Nitrogen availability and TOR
639 regulate the Snf1 protein kinase in *Saccharomyces cerevisiae*. Eukaryot Cell.
640 2006;5(11):1831-7.
641 18. Lin SS, Manchester JK, Gordon JI. Sip2, an N-myristoylated beta subunit of
642 Snf1 kinase, regulates aging in *Saccharomyces cerevisiae* by affecting cellular histone
643 kinase activity, recombination at rDNA loci, and silencing. J Biol Chem.
644 2003;278(15):13390-7.
645 19. Wierman MB, Maqani N, Strickler E, Li M, Smith JS. Caloric Restriction
646 Extends Yeast Chronological Life Span by Optimizing the Snf1 (AMPK) Signaling
647 Pathway. Mol Cell Biol. 2017;37(13).
648 20. Wang Z, Wilson WA, Fujino MA, Roach PJ. Antagonistic controls of autophagy
649 and glycogen accumulation by Snf1p, the yeast homolog of AMP-activated protein
650 kinase, and the cyclin-dependent kinase Pho85p. Mol Cell Biol. 2001;21(17):5742-52.
651 21. Wright RM, Poyton RO. Release of two *Saccharomyces cerevisiae* cytochrome
652 genes, COX6 and CYC1, from glucose repression requires the SNF1 and SSN6 gene
653 products. Mol Cell Biol. 1990;10(3):1297-300.
654 22. Mi H, Muruganujan A, Casagrande JT, Thomas PD. Large-scale gene function
655 analysis with the PANTHER classification system. Nat Protoc. 2013;8(8):1551-66.
656 23. Dilova I, Easlon E, Lin SJ. Calorie restriction and the nutrient sensing signaling
657 pathways. Cell Mol Life Sci. 2007;64(6):752-67.
658 24. Morselli E, Maiuri MC, Markaki M, Megalou E, Pasparaki A, Palikaras K, et al.
659 Caloric restriction and resveratrol promote longevity through the Sirtuin-1-dependent
660 induction of autophagy. Cell Death Dis. 2010;1:e10.
661 25. Cheong H, Yorimitsu T, Reggiori F, Legakis JE, Wang CW, Klionsky DJ. Atg17
662 regulates the magnitude of the autophagic response. Mol Biol Cell.
663 2005;16(7):3438-53.
664 26. Sia RA, Mitchell AP. Stimulation of later functions of the yeast meiotic protein
665 kinase Ime2p by the IDS2 gene product. Mol Cell Biol. 1995;15(10):5279-87.
666 27. Neuberger G, Schneider G, Eisenhaber F. pkaPS: prediction of protein kinase A
667 phosphorylation sites with the simplified kinase-substrate binding model. Biol Direct.
668 2007;2:1.
669 28. Sharmin D, Sasano Y, Sugiyama M, Harashima S. Effects of deletion of different
670 PP2C protein phosphatase genes on stress responses in *Saccharomyces cerevisiae*.
671 Yeast. 2014;31(10):393-409.
672 29. Liu PJ, Chen CD, Wang CL, Wu YC, Hsu CW, Lee CW, et al. In-depth

673 proteomic analysis of six types of exudative pleural effusions for nonsmall cell lung
674 cancer biomarker discovery. Molecular & cellular proteomics : MCP.
675 2015;14(4):917-32.
676 30. Schopf FH, Biebl MM, Buchner J. The HSP90 chaperone machinery. Nat Rev
677 Mol Cell Biol. 2017;18(6):345-60.
678 31. Li J, Soroka J, Buchner J. The Hsp90 chaperone machinery: conformational
679 dynamics and regulation by co-chaperones. Biochim Biophys Acta.
680 2012;1823(3):624-35.
681 32. Richter K, Walter S, Buchner J. The Co-chaperone Sba1 connects the ATPase
682 reaction of Hsp90 to the progression of the chaperone cycle. J Mol Biol.
683 2004;342(5):1403-13.
684 33. Wolmarans A, Lee B, Spyracopoulos L, LaPointe P. The Mechanism of Hsp90
685 ATPase Stimulation by Aha1. Sci Rep. 2016;6:33179.
686 34. Francis BR, Thorsness PE. Hsp90 and mitochondrial proteases Yme1 and
687 Yta10/12 participate in ATP synthase assembly in *Saccharomyces cerevisiae*.
688 Mitochondrion. 2011;11(4):587-600.
689 35. Wang Y, Singh U, Mueller DM. Mitochondrial genome integrity mutations
690 uncouple the yeast *Saccharomyces cerevisiae* ATP synthase. J Biol Chem.
691 2007;282(11):8228-36.
692 36. Distel B, Gould, SJ., Voorn-Brouwer, T., van der Berg, M., Tabak, HF.,
693 Subramani, S. The carboxyl-terminal tripeptide serine-lysine-leucine of firefly
694 luciferase is necessary but not sufficient for peroxisomal import in yeast. New Biol.
695 1992;4(2):157-65.
696 37. Chiti F, Dobson CM. Protein Misfolding, Amyloid Formation, and Human
697 Disease: A Summary of Progress Over the Last Decade. Annu Rev Biochem.
698 2017;86:27-68.
699 38. O'Connell JD, Tsechansky M, Royal A, Boutz DR, Ellington AD, Marcotte EM.
700 A proteomic survey of widespread protein aggregation in yeast. Mol Biosyst.
701 2014;10(4):851-61.
702 39. Franzosa EA, Albanese V, Frydman J, Xia Y, McClellan AJ. Heterozygous yeast
703 deletion collection screens reveal essential targets of Hsp90. PLoS One.
704 2011;6(11):e28211.
705 40. Yang X, Zhang Y, Xu W, Deng R, Liu Y, Li F, et al. Potential role of Hsp90 in rat
706 islet function under the condition of high glucose. Acta Diabetol. 2016;53(4):621-8.
707 41. Lei H, Venkatakrishnan A, Yu S, Kazlauskas A. Protein kinase A-dependent
708 translocation of Hsp90 alpha impairs endothelial nitric-oxide synthase activity in high
709 glucose and diabetes. J Biol Chem. 2007;282(13):9364-71.
710 42. Verna J, Lodder A, Lee K, Vagts A, Ballester R. A family of genes required for

maintenance of cell wall integrity and for the stress response in *Saccharomyces cerevisiae*. Proc Natl Acad Sci U S A. 1997;94(25):13804-9.

43. Petkova MI, Pujol-Carrion N, Arroyo J, Garcia-Cantalejo J, Angeles de la Torre-Ruiz M. Mtl1 is required to activate general stress response through Tor1 and Ras2 inhibition under conditions of glucose starvation and oxidative stress. J Biol Chem. 2010;285(25):19521-31.

44. Arino J, Casamayor A, Gonzalez A. Type 2C protein phosphatases in fungi. Eukaryot Cell. 2011;10(1):21-33.

45. Warmka J, Hanneman J, Lee J, Amin D, Ota I. Ptc1, a type 2C Ser/Thr phosphatase, inactivates the HOG pathway by dephosphorylating the mitogen-activated protein kinase Hog1. Mol Cell Biol. 2001;21(1):51-60.

46. Aluru M, McKinney T, Venero AL, Choudhury S, Torres M. Mitogen-activated protein kinases, Fus3 and Kss1, regulate chronological lifespan in yeast. Aging (Albany NY). 2017;9(12):2587-609.

47. Ali MM, Roe SM, Vaughan CK, Meyer P, Panaretou B, Piper PW, et al. Crystal structure of an Hsp90-nucleotide-p23/Sba1 closed chaperone complex. Nature. 2006;440(7087):1013-7.

48. Rohl A, Rohrberg J, Buchner J. The chaperone Hsp90: changing partners for demanding clients. Trends Biochem Sci. 2013;38(5):253-62.

49. Meyer P, Prodromou C, Liao C, Hu B, Roe SM, Vaughan CK, et al. Structural basis for recruitment of the ATPase activator Aha1 to the Hsp90 chaperone machinery. EMBO J. 2004;23(6):1402-10.

50. Wang YT, Tsai CF, Hong TC, Tsou CC, Lin PY, Pan SH, et al. An informatics-assisted label-free quantitation strategy that depicts phosphoproteomic profiles in lung cancer cell invasion. Journal of proteome research. 2010;9(11):5582-97.

51. Kanehisa M, and Susumu Goto. KEGG: Kyoto Encyclopedia of Genes and Genomes. Nucleic Acids Research. 2000;28(1):27-30.

52. Portela P, Howell S, Moreno S, Rossi S. In vivo and in vitro phosphorylation of two isoforms of yeast pyruvate kinase by protein kinase A. J Biol Chem. 2002;277(34):30477-87.

53. Roskoski R. Assays of protein kinase. Methods in Enzymology. 1983;99:3-6.

54. Vizcaino JA, Deutsch EW, Wang R, Csordas A, Reisinger F, Rios D, et al. ProteomeXchange provides globally coordinated proteomics data submission and dissemination. Nat Biotechnol. 2014;32(3):223-6.

55. Ashburner M, Ball CA, Blake JA, Botstein D, Butler H, Cherry JM, Davis AP, Dolinski K, Dwight SS, Eppig JT, Harris MA, Hill DP, Issel-Tarver L, Kasarskis A, Lewis S, Matese JC, Richardson JE, Ringwald M, Rubin GM, Sherlock G. Gene

749 ontology: tool for the unification of biology. The Gene Ontology Consortium. Nature
750 genetics. 2000;25(1):25-49.
751 56. Dennis G Jr1 SB, Hosack DA, Yang J, Gao W, Lane HC, Lempicki RA. DAVID:
752 Database for Annotation, Visualization, and Integrated Discovery. Genome Biol.
753 2003;4(5):3.
754 57. Postnikoff SD, Harkness TA. Replicative and chronological life-span assays.
755 Methods Mol Biol. 2014;1163:223-7.
756 58. Longo VD, Shadel GS, Kaeberlein M, Kennedy B. Replicative and chronological
757 aging in *Saccharomyces cerevisiae*. Cell Metab. 2012;16(1):18-31.
758 59. Smith DL, Jr., McClure JM, Matecic M, Smith JS. Calorie restriction extends the
759 chronological lifespan of *Saccharomyces cerevisiae* independently of the Sirtuins.
760 Aging Cell. 2007;6(5):649-62.
761 60. Tsai CF, Wang YT, Chen YR, Lai CY, Lin PY, Pan KT, et al. Immobilized metal
762 affinity chromatography revisited: pH/acid control toward high selectivity in
763 phosphoproteomics. Journal of proteome research. 2008;7(9):4058-69.
764 61. Toone WM, Jones N. Stress-activated signalling pathways in yeast. Genes to
765 cells : devoted to molecular & cellular mechanisms. 1998;3(8):485-98.
766 62. French JB, Zhao H, An S, Niessen S, Deng Y, Cravatt BF, et al. Hsp70/Hsp90
767 chaperone machinery is involved in the assembly of the purinosome. Proc Natl Acad
768 Sci U S A. 2013;110(7):2528-33.
769 63. Sievers F, Higgins DG. Clustal omega. Curr Protoc Bioinformatics. 2014;48:3 13
770 1-6.

771

772

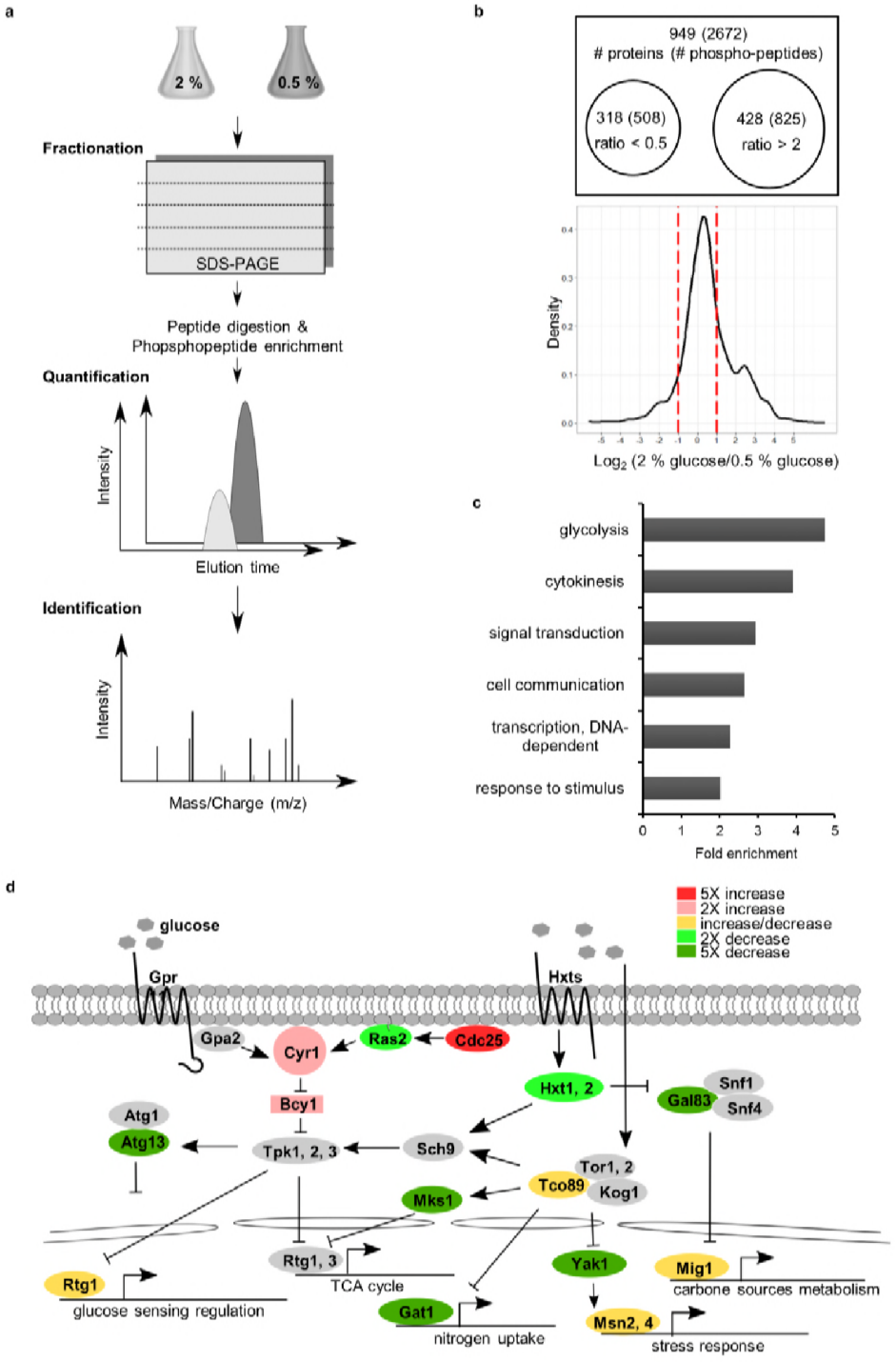

773

774 **S1 Fig. The strategy used for large-scale identification of CR-modulated**

775 **pathways**.

776 **a**, Experimental workflow for quantitative proteomics-identified CR-regulated

proteins in yeast. **b**, Venn diagrams represent the increased abundance of phosphorylated peptides (proteins) under normal conditions compared to CR by over 50 % ($\log_2 > 1$) or the decreased abundance of phosphorylated peptides (proteins) under normal conditions versus CR treatment by over 50 % ($\log_2 < -1$). The distribution of $\log_2$ (2 % glucose / 0.5 % glucose) ratios for phosphopeptides are illustrated by a density plot. **c**, GO term analysis of phosphorylated proteins regulated by CR. The top 6 enriched biological processes are shown. **d**, Some phosphoproteins regulated by CR are factors in the glucose-sensing pathway. The phosphoproteins with a greater than 2-fold change are labelled with different colors to indicate their ratios. The phosphoproteins containing both phosphorylation and dephosphorylation sites under CR are labelled in yellow.

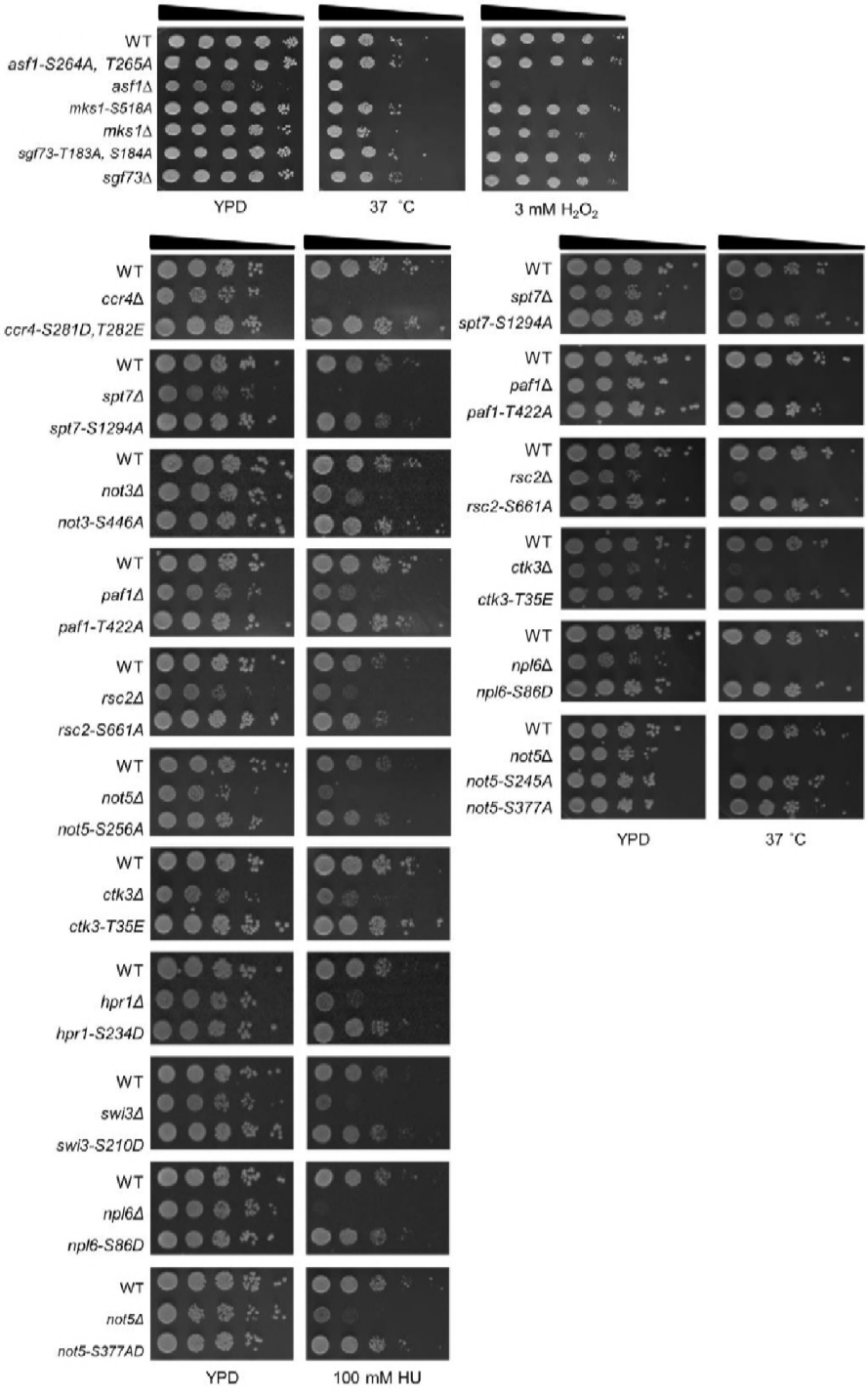

S2 Fig. Most phosphorylation site mutants displayed wild-type phenotypes under stress conditions.

Phosphorylation site mutants as indicated were spotted onto YPD plates. Images were

taken after 3 days under different stresses. Of the 53 phosphorylation site mutants, only some representative examples are shown here.

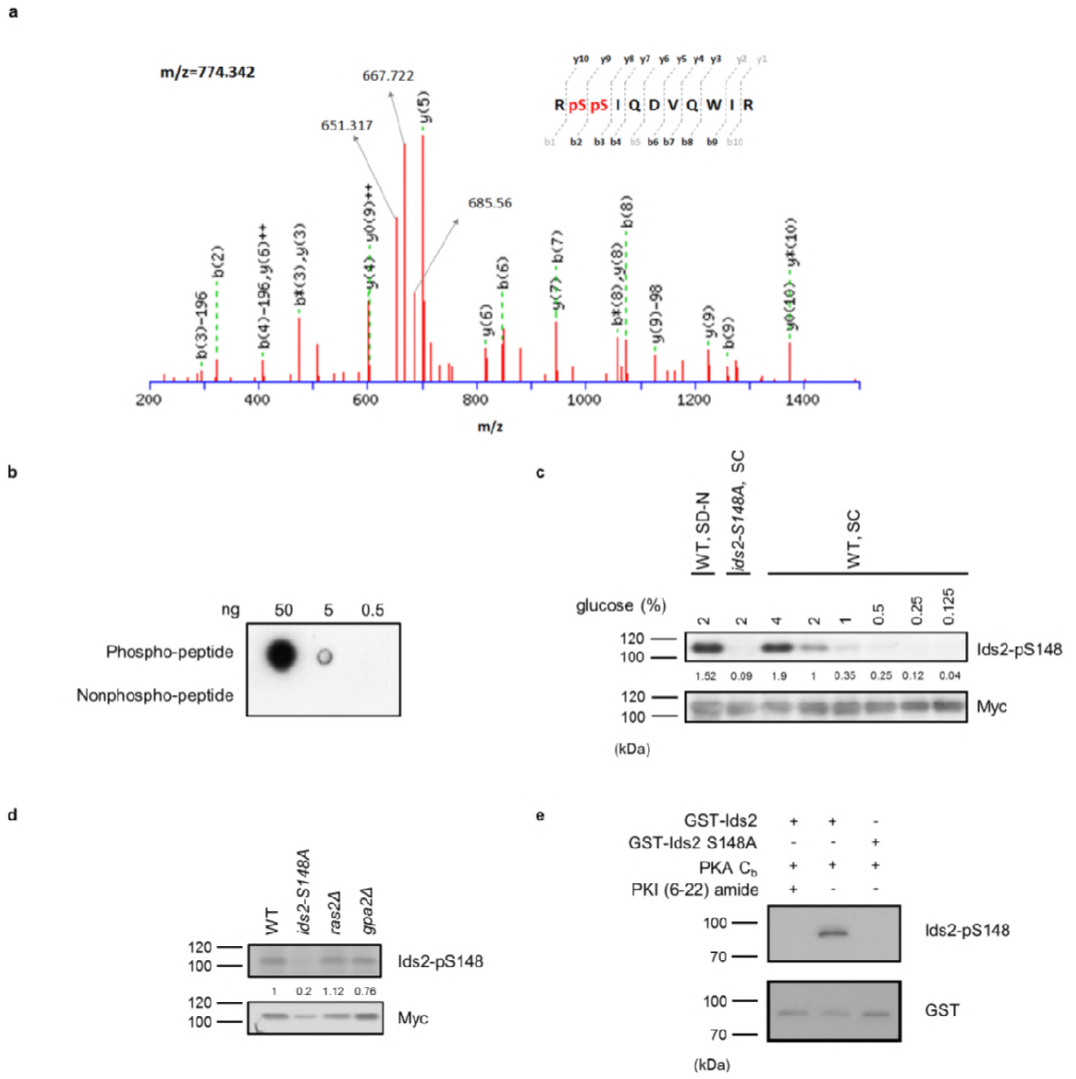

S3 Fig. Characterization of the phosphospecific antibodies against Ids2 S148.

a, The mass spectrum of the phosphopeptide Ids2 S148 recorded in the linear mode. **b**, Peptide spotting showed the specificity of the phospho-Ids2-S148 antibodies. **c**, The phosphorylation level of Ids2-S148 under different conditions. The WT strain was transformed with pRS426-Ids2-Myc_{13} (WT) or pRS426-Ids2-S148A-Myc_{13} (*ids2*-S148A). Overnight cultures of these strains were refreshed to OD_{600} = 0.3 in SC-Ura with 4%, 2%, 1%, 0.5%, 0.25%, and 0.125 % glucose for 3 hours. For

804 nitrogen starvation, the overnight culture was refreshed to OD_{600} = 0.3 in SC-Ura with
805 2% glucose for 3 hours and then transferred to SC medium lacking nitrogen (SD-N)
806 with 2% glucose for 2 hours. Cell lysates were prepared for Western blot analysis. The
807 numbers below are the intensity ratios of Ids2-p148/Myc compared with those of WT.
808 **d**, WT and deletion strains were transformed with pRS426-Ids2-$Myc_{13.}$ Cells were
809 grown in SC medium with 2% glucose, and lysates were prepared for Western blot
810 analysis. e, In vitro PKA activity was assayed using bovine heart catalytic subunit C
811 (C_b), and the PKA inhibitor PKI 6-22 was used as a negative control. GST-Ids2 and
812 GST-Ids2-S148A served as substrates. Activities were detected by Western blot
813 analysis using the phosphospecific antibody. The total amount of Ids2 protein was
814 detected by a GST antibody.

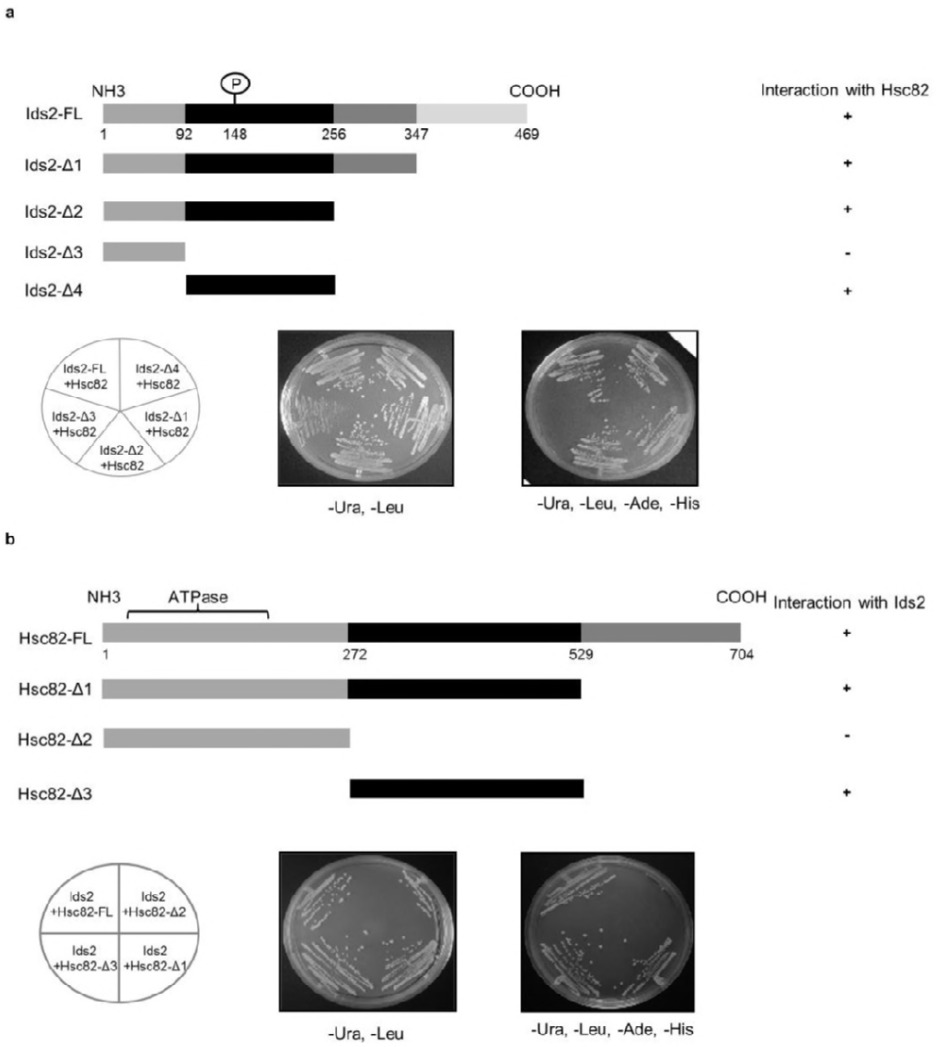

S4 Fig. Mapping the interacting domains between Ids2 and Hsc82 by the yeast two-hybrid assay.

a, The upper panel shows a schematic diagram of various pGBDU-Ids2 truncations. The two-hybrid assay was conducted using various truncated Ids2 proteins as the bait and full-length Hsc82 as the prey. Cells were restreaked onto SC-Leu-Ura-Ade-His glucose plates to investigate the bait-prey reciprocity. **b**, The upper panel depicts a

schematic diagram of various Hsc82 truncations. The assay was conducted as described in **a** to define the Ids2-Hsc82 interaction domain in Hsc82.

826

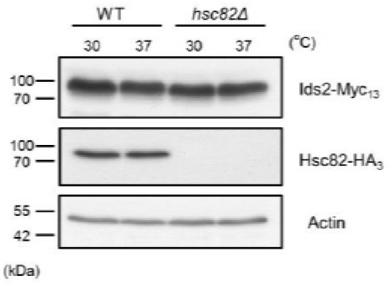

827

828 **S5 Fig. The effect of heat-shock stress or *hsc82Δ* on the protein levels of Ids2.**

829 Chromosomally tagged Ids2-Myc_{13} and Hsc82-HA_3 strains were cultured under

830 normal (30 °C) or heat-shock (37 °C) conditions for 3 hours. Cell lysates were

831 examined by Western blot analysis using Myc or HA antibodies. Actin served as a

832 loading control.

833

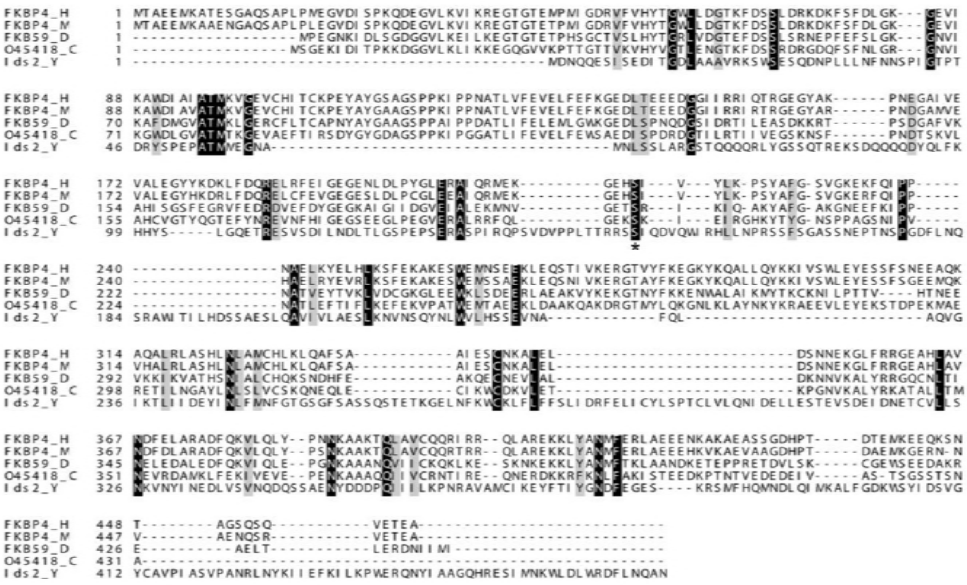

834

S6 Fig. An alignment of Ids2 and its homologs.

Multiple sequence alignment was performed between Ids2 and its predicted homologues by Clustal Omega program (63). S148 of Ids2 is marked with an asterisk. H, *Homo sapiens*; M, *Mus musculus*; D, *Drosophila melanogaster*; C, *Caenorhabditis elegans*: Y, *Saccharomyces cerevisiae*.

S1 Data. The list of total phosphopeptides influenced by calorie restriction.

S2 Data. Genes and mutation sites for functional screening.

S3 Data. A list of peptides detected from Mass Spectrometry analysis of the Ids2-TAP co-purified proteins.

S4 Data. Yeast strains, plasmids, and primer sets used in this study.

Acknowledgements

We thank Prof. Silvia Rossi for yeast strains. We also thank Chia-Feng Tsai for his assistance of mass spectrometry analysis. This work was financially supported by the "Center of Precision Medicine" from The Featured Areas Research Center Program within the framework of the Higher Education Sprout Project by the Ministry of Education (MOE) and the Ministry of Science and Technology (MOST 106-2311-B-002-010-MY3) in Taiwan.

Contributions

Y.-C.C., P.-H.J., H.-M.C., C.-H.C., Y.-T.W., and C.-J.Y. conducted and analyzed the experiments. Y.-C.C., P.-H.J., Y.-J.C., C.-J.Y., and S.-C.T. designed the experiments and interpreted the data. Y.-C.C., P.-H.J., H.-M.C., and S.-C.T. edited the manuscript. S.-C.T. conceived and supervised this study.

Competing interests

The authors declare no competing financial interests.